Incorporation of manganese into semiconducting ScN using radio frequency molecular beam epitaxy

Hamad A. AL-Brithen, Haiqiang Yang, and Arthur R. Smith[a)]
Condensed Matter and Surface Science Program, Department of Physics and Astronomy, Ohio University, Athens, Ohio 45701

(Received 23 March 2004; accepted 12 July 2004)

The incorporation of manganese into semiconducting ScN, using radio frequency molecular beam epitaxy, has been investigated. X-ray diffraction and reflection high energy electron diffraction measurements show the face-centered tetragonal rocksalt-type crystal structure with Sc and Mn cations and N anions. In addition to the solute incorporation into the lattice, which is clear from the positions of the diffraction peaks, atomic force microscopy images show that the surface of the alloy grown at $T_S \leqslant 518$ °C contains dot-like features, indicating surface accumulation. The areal dot density is found to decrease as the growth temperature increases, whereas the Mn incorporation increases at 518 °C. This behavior is suggestive of a thermally activated process, and it is well explained by an Arrhenius law, giving an activation energy (diffusion barrier) of 0.67 eV. Increasing the growth temperature to 612 °C leads to an increased desorption rate, resulting in little Mn incorporation. It has been found that the growth is nearly optimized at $T_S = 518$ °C for high Mn incorporation, smooth growth, and small accumulate density. The alloy is found to have lattice parameters which depend on the Mn/(Mn+Sc) bulk ratio. The alloy lattice constants follow Vegard's law depending on the Mn bulk fraction and the lattice constants of ScN and θ-phase MnN. The Mn incorporation and Mn incorporation coefficient for films grown at $T_S = 518$ °C increase as the Mn/(Mn+Sc) flux ratio increases. © *2004 American Institute of Physics*. [DOI: 10.1063/1.1788842]

I. INTRODUCTION

It is currently of great interest to dope III–V semiconductors, such as GaAs and GaN, with transition metal magnetic dopants, such as Mn and Cr, for the purpose of forming a dilute magnetic semiconductor. The GaN system in particular became of high interest due to the prediction of T_C in MnGaN above 300 K.[1] However, transition metals, including Mn and Cr, commonly adopt octahedral bonding configurations with N rather than tetrahedral.[2–4] This dissimilarity may contribute to problems with growth, including difficulties with incorporation and also precipitation of Mn or Mn_xN_y phases in MnGaN. As a characteristic of the dissimilar bonding configurations (nonisocrystallinity) MnGaN does not clearly follow Vegard's law.[5] It is therefore of interest to find a semiconductor system which is octahedral and which may therefore be easily doped with Mn. One such possibility is ScN.

Transition metal nitrides (TMNs) such as ScN have been studied in recent years for their unique physical properties including high hardness, high temperature stability, mechanical strength, off-stoichiometry, magnetic properties, and electronic transport properties that vary from semiconductors to metals.[2–4,6–21]

ScN is expected to have novel applications of its own. ScN stabilizes in rocksalt structure, having octahedral bonding, with a lattice constant $a_{ScN} = 4.503$ Å, hardness $H = 21$ GPa, and melting point $T_m \sim 2600$ °C. Moreover, ScN exhibits an optical gap at $E_g \sim 2.15$ eV and a lower energy gap at ~0.9 eV.[11–15,18,22–28] The smooth and epitaxial growth of ScN(001) on MgO(001) was achieved at temperature (T_S) of 800 °C by radio frequency molecular beam epitaxy (rf MBE).[13,14,28]

MnN forms a face-centered tetragonal (fct) structure exhibiting antiferromagnetic behavior at room temperature.[2,10] Yang *et al.* reported the growth of MnN(001) on MgO(001) using rf N-plasma MBE at T_S over the range of 250–450 °C, finding the lattice constants of this material to be $a_{MnN} = b_{MnN} = 4.22$ Å and $c_{MnN} = 4.12$ Å.[3] Also, reflection high electron energy diffraction (RHEED) of MnN(001) indicated the growth is smooth at $T_S = 450$ °C.

It is well known for MBE growth of ternary alloys that the growth temperature and flux ratios affect the incorporation, precipitation, and adatom desorption even in the case of an isocrystalline alloy system.[5,29,30] For example, for the case of doping GaN with Mg, increasing the growth temperature over the range 600–700 °C results in an exponential reduction of Mg incorporation.[31] As another example, incorporation of several percent Mn in GaAs must be done at low temperature to avoid precipitation of MnAs. In this case, a low growth temperature allows one to incorporate several percent of Mn, but usually a lot of interstitial Mn is present, i.e., not all Mn substitutes for Ga. At higher growth temperature, the maximum Mn content, before precipitation sets in, is lower, but usually interstitial Mn is avoided. There is clearly a balance of rates which takes place, including incident flux rate R_f, incorporation rate R_i, surface desorption rate R_d, and surface accumulation rate R_a. Since atoms which land on the surface can either incorporate at a lattice or in-

a)Author to whom correspondence should be addressed.

terstitial site, desorb from the surface, or accumulate on the surface, we have the rate equation $R_f = R_i + R_d + R_a$. Clearly, it is necessary to investigate how these rates are affected by the growth conditions in order to optimize the structural, magnetic, and electronic properties of the alloy.

In this paper, we report the growth of MnScN by rf MBE. Our study is mainly focused on the investigation of the structural properties. In the first section, the Mn incorporation and crystalline symmetry are discussed, as well as the surface smoothness, accumulation, and desorption as a function of the sample growth temperature T_S. In the second section, alloy lattice parameters and Mn incorporation as a function of Mn/(Mn+Sc) flux ratio R and Mn/(Mn+Sc) bulk ratio x are presented.

II. EXPERIMENTAL PROCEDURE

MnScN layers are grown by rf MBE on ScN(001)/MgO(001) substrates, using a radio frequency N-plasma source for nitrogen and effusion cells for both scandium and manganese. MgO (001) substrates are first cleaned with solvents, then loaded into the MBE chamber and heated up to ~1000 °C for 30 min with nitrogen plasma applied.[14,28]

Prior to the growth of MnScN, growth of a ScN (001) buffer layer, under N-rich conditions, on MgO (001) takes place with $T_S \sim 800$ °C and the pressure of nitrogen and plasma source power set at 1.1×10^{-5} Torr and 500 W, respectively; the effective N flux for the stated conditions is $\sim 3.6\times10^{14}$ cm^{-2} s^{-1}.[14,28] The Sc flux, determined using a crystal thickness monitor, is 1.14×10^{14} cm^{-2} s^{-1}, and the buffer layer thickness is ~600 Å.

After the growth of ScN(001)/MgO(001), T_S is reduced to a value in the range 330–612 °C, after which the growth of the MnScN alloy began. Sc and N flux are kept the same as for the buffer layer growth. Two types of growth parameter studies were performed. First, MnScN films were grown with fixed $R = 19\%$ but different T_S. Second, MnScN films were grown with fixed $T_S = 518$ °C but different R. The growth time for both sets of MnScN films is about 120 min, resulting in MnScN layer thicknesses in the range 1700–2000 Å.

The growth is monitored using RHEED with electron energy =20 keV. *Ex situ* x-ray diffraction (XRD) measurements, using Cu K_α x-rays, and atomic force microscopy (AFM) imaging are performed. Peak fitting is used to determine the XRD peak positions and RHEED pattern streak spacings. The XRD, RHEED, and AFM results are employed to study the crystal symmetry, surface smoothness and morphology, and lattice constants of the MnScN alloy.

III. RESULTS AND DISCUSSION

A. MnScN alloys grown at different temperatures with the same Mn/(Mn+Sc) flux ratio *R*

Figure 1 shows the XRD spectrum of the MnScN film grown at $T_S = 330$ °C and the alloy peak position as a function of the growth temperature for $R = 19\%$. In Fig. 1(a), three peaks are seen at $2\theta = 39.98°$, 40.56°, and 42.95°. The first and third peaks are attributed to ScN 002 and MgO 002,

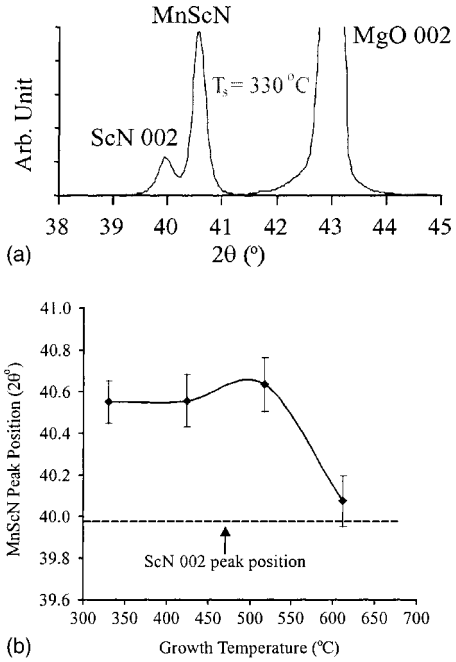

FIG. 1. (a) XRD spectrum of MnScN on ScN(001)/MgO(001) grown at 330 °C; (b) the XRD peak position of the MnScN alloy as a function of the growth temperature.

respectively, for the following three reasons. First, their positions do not vary with the change of the growth parameters. Second, the peak intensities agree with the thickness of each film, small for the buffer layer ScN 002 and very high for the substrate MgO 002. Third, the corresponding lattice constants from their peak positions (4.512 Å for ScN and 4.213 Å for MgO) agree well with the known values of 4.503 and 4.213 Å, respectively (note spectrum is calibrated to MgO 002).[13,14,23,28] The middle peak at $2\theta = 40.56°$ has not been seen in ScN(001)/MgO(001) films which we have previously reported and consequently is attributed to the MnScN alloy.[13,14,28] Similar MnScN spectra have been observed for growth at $T_S = 424$, 518, and 612 °C. Since XRD of each film shows only one peak for the alloy (plus the higher orders, not shown), this indicates that MnScN forms a crystalline layer with 001 orientation.

Figure 1(b) shows the XRD peak position of the alloy as a function of T_S. What can be seen is that for the two lowest values of T_S, the position of the alloy peak (thus the Mn incorporation) is about the same. At $T_S = 518$ °C, the alloy peak is shifted further away from that of ScN 002, indicating a slight increase in Mn incorporation. Finally, at $T_S = 612$ °C, the Mn incorporation is considerably reduced.

The symmetry of the alloy surface structures has been examined by RHEED. Figure 2 presents the RHEED patterns of MnScN grown at different temperatures acquired along [010] and [110]. The patterns of all films show fourfold 1×1 surface symmetry with no reconstruction and are similar to the RHEED patterns of ScN(001),[6,14,28] indicating the rocksalt-type of the alloy surface unit cell. This means that the alloy has a fct crystal structure with $[010]_{MnScN} \| [010]_{ScN}$ and $[110]_{MnScN} \| [110]_{ScN}$ and thus grows epitaxially on ScN(001). The fact that the alloy lattice constants get smaller

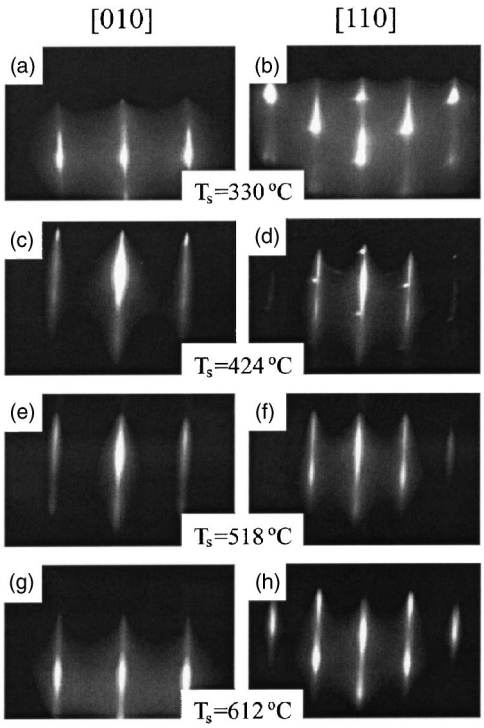

FIG. 2. RHEED patterns of MnScN films grown at different sample temperatures (T_S) acquired along both [010] and [110] directions of ScN(001).

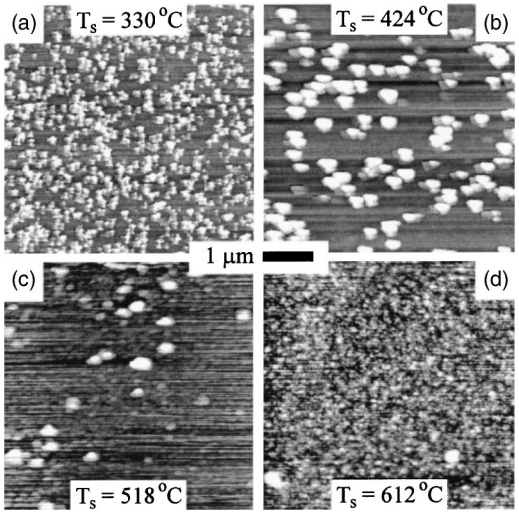

FIG. 3. AFM images of MnScN films as a function of the growth temperature. Each image size is 5×5 μm^2. The gray scale of the images shown in (a)–(d) are 135, 150, 80, and 40 Å, respectively; moreover, the root mean square (r.m.s.) roughness of the surfaces are 40, 50, 15, and 10 Å, respectively. Note: dark horizontal bands in the images are due to a line-by-line background subtraction.

compared with ScN shows that the Mn atoms are not in interstitial sites but rather are on the Sc sites.

The rf MBE growth of ScN(001) under N-rich conditions requires a high growth temperature, T_S=800 °C, in order to achieve a film with a smooth surface;[14,28] however, attaining two-dimensional growth of fct MnN(001) can be achieved at T_S=450 °C.[3] This indicates that adatoms on the MnN surface have smaller surface diffusion barrier comparing with adatoms on ScN(001). It is interesting that for the alloy, fairly streaky RHEED patterns are obtained at temperatures comparable to those used for MnN.

Although RHEED of all films, shown in Fig. 2, is generally streaky, spots and weak rings are observed. For the film grown at T_S=330 °C, the RHEED patterns show segmented streaks and spots, which indicates some roughness on the surface. RHEED patterns of the film grown at T_S =424 °C are streakier, exhibiting smaller spots and some faint rings. The reduction of the spot size indicates improved surface smoothness although the rings are indicative of some polycrystalline structure existing on the surface (Note: this is due to surface accumulation, to be discussed). For the case of the growth at T_S=518 °C, RHEED shows streakier patterns, and rings are hardly visible. Increasing the growth temperature to T_S=612 °C, the surface of the MnScN shows more segmented streaks, indicating increased surface roughness.

In order to investigate the surface structure in real space, AFM imaging has been performed, as shown in Fig. 3 for different growth temperatures. The size of each image is 5 $\times5$ μm^2.

In Figs. 3(a)–3(c) the AFM images show that the MnScN surface is covered with a certain density of sub-μm-sized dot-like structures, which are suggestive of surface accumulation. Quantitatively, these dots [In Fig. 3(a)] form a layer of average thickness 130 Å, compared to the MnScN layer thickness of 2000 Å; thus the dots have a volume less than 7% of that of the MnScN film. Interestingly, their areal density σ is reduced considerably as the growth temperature is increased. This trend is consistent with the RHEED, which shows the most streaky pattern at 518 °C. The rings and spots in the RHEED patterns for growth at $T_S\leqslant$518 °C are therefore attributed to these dot features. For the case of growth at T_S=330 °C, the dot density is very large, yet the size of each dot is small. At T_S=424 °C, the dot density is smaller but the dot size is larger, resulting in the largest r.m.s. roughness of the four surfaces shown. For growth at T_S =518 °C, the dot density is reduced further, but the dot sizes are not larger than at 424 °C, which is attributed to increased evaporation. Negligible dot density is observed for growth at T_S=612 °C, but the surface shows an r.m.s. roughness of 9.9 Å, consistent with ScN(001) layers grown at low temperature.

This behavior is consistent with a thermally activated process. For example, at low T_S, the diffusion length and surface desorption are limited, which results in more numerous, but smaller dots (accumulates). At higher T_S, the diffusion length is increased, leading to the formation of fewer, but larger, dots (accumulates). The thermally activated process of the surface diffusion is described by an Arrhenius law[32]

$$N = \omega_A e^{-E_B/k_B T}, \tag{1}$$

where N is the average number of hops per unit time interval, ω_A is the atomic oscillation frequency (attempt frequency), and E_B is the surface diffusion barrier. The diffusion length L is proportional to the square root of N. Accordingly, L increases as the temperature increases, leading to a reduction of the areal dot density, an increase of the dot size, and an improvement in the surface smoothness. Smaller incorporation at T_S=612 °C is due to increased desorption.

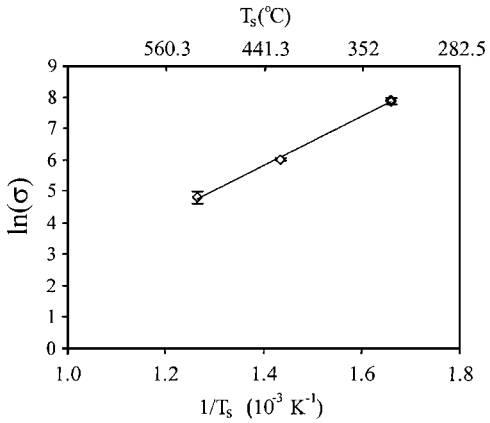

FIG. 4. The natural logarithm of the areal dot density as a function of the inverse growth temperature.

Since the Mn incorporation is roughly constant for $T_S < 518$ °C and only a little larger at $T_S = 518$ °C, as indicated by the XRD results [Fig. 1(b)], the surface diffusion barrier E_B is considered constant. Assuming the areal dot density σ is inversely proportional to the square of the diffusion length L^2, which is as mentioned proportional to the average number of hops per unit time N, the following relation is obtained

$$\ln(\sigma) = C + \frac{E_B}{k_B}\frac{1}{T_s}, \tag{2}$$

where C is a constant.

In Fig. 4, the natural logarithm of the number of accumulates per 100 μm^2 vs the inverse of the growth temperature is plotted. As can be seen, the relation is quite linear. The slope of the fitted line is (E_B/k_B), according to Eq. (2). From this, the calculated diffusion barrier is about 0.67 eV. This value compares well with values of diffusion barriers on other nitride surfaces. For example, in the case of GaN, the diffusion barriers of the Ga adatom on N-terminated (Ga-terminated) GaN(0001) and GaN(000$\bar{1}$) are 1.8 (0.4) and 1.0 (0.2) eV, respectively.[33] Therefore, the diffusion barrier of 0.67 eV for the nonpolar surface, MnScN(001), has an intermediate value between the Ga- and N-terminated wurtzite GaN{0001} surfaces, which are polar.

Growth of MnScN(001) is approximately optimized at $T_S = 518$ °C to achieve high Mn incorporation, smooth surface, and low density of accumulates, as indicated by XRD, RHEED, and AFM, respectively. In the following section, the growth of MnScN at $T_S = 518$ °C with different R for each film is presented.

B. Epitaxial growth of MnScN with different Mn/(Mn+Sc) flux ratios

Figure 5 shows the XRD spectra of MnScN grown on ScN(001) at $T_S = 518$ °C with different R. The Mn/(Mn+Sc) flux ratios for films of Fig. 5(a), 5(b), and 5(c) are 10%, 19%, and 26%, respectively. The three peaks ScN 002, MgO 002, and MnScN 002 are clearly evident. For $R = 10\%$, the alloy peak overlaps with the ScN peak. At higher flux ratios, the alloy peak is shifted further to the right of the ScN peak.

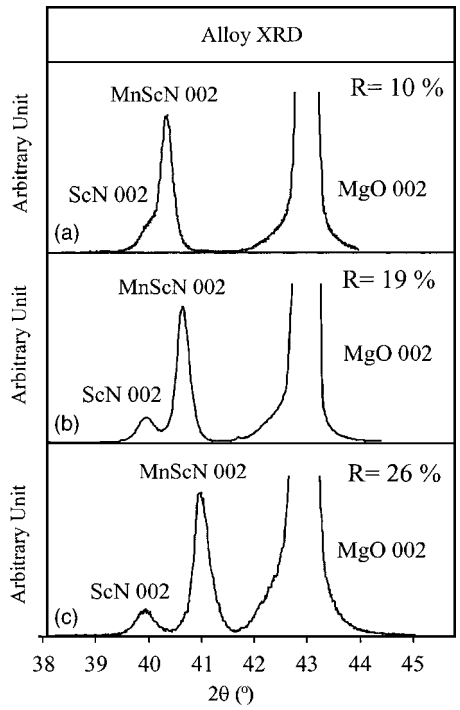

FIG. 5. XRD spectra of MnScN grown at $T_S = 518$ °C at different Mn/(Mn+Sc) flux ratios: (a) 10%; (b) 19%; and (c) 26%.

The increase of the angle of MnScN 002 peak with increasing R indicates a reduction of the alloy vertical lattice constant c_{alloy}, indicating increased Mn incorporation when R increases.

The surface structure of MnScN(001) has been investigated by RHEED. Figures 6(a)–6(c) show the RHEED patterns along [010] of MnScN(001) grown at $T_S = 518$ °C, R of each surface is given. Furthermore, Fig. 6(d) shows the plot of the averaged-line profiles of the right streak of each RHEED pattern as a function of the distance from the midpoint of the corresponding left streak.

RHEED of all films shown in Fig. 6 shows fourfold symmetry of the surfaces and streaky patterns, consistent with our observations in the preceding section. No reconstruction besides 1×1 is seen for any surface. It is seen from Fig. 6(d) that the spacing between the streaks increases as Mn flux is increased, corresponding to a decrease in the *in-plane* lattice constants (a_{alloy} *and* b_{alloy}). The reduction of the lattice parameters as R increases is also indicated by XRD, as mentioned, and is attributed to the increased Mn bulk fraction.

To calculate c_{alloy}, we use Bragg's law. For the calculation of a_{alloy}, the spacing between the main streaks of the alloy RHEED patterns along [010] (d_{alloy}) is compared with the spacing between the main streaks of ScN(001) along the same direction d_{ScN}. As is well known, d_{alloy} and d_{ScN} are proportional to the reciprocal lattice constants of the alloy and ScN, respectively; therefore, the ratio of streak spacings $(d_{\text{alloy}}/d_{\text{ScN}})$ is equal to the reciprocal ratio of the real lattice constants, $(a_{\text{alloy}}/a_{\text{ScN}}) = (d_{\text{ScN}}/d_{\text{alloy}})$. As a result, a_{alloy} is extracted.[34]

Applying Vegard's law considering the known lattice constants of ScN and θ-phase MnN as well as the measured lattice parameters of the alloy, the Mn/(Mn+Sc) bulk ratio x

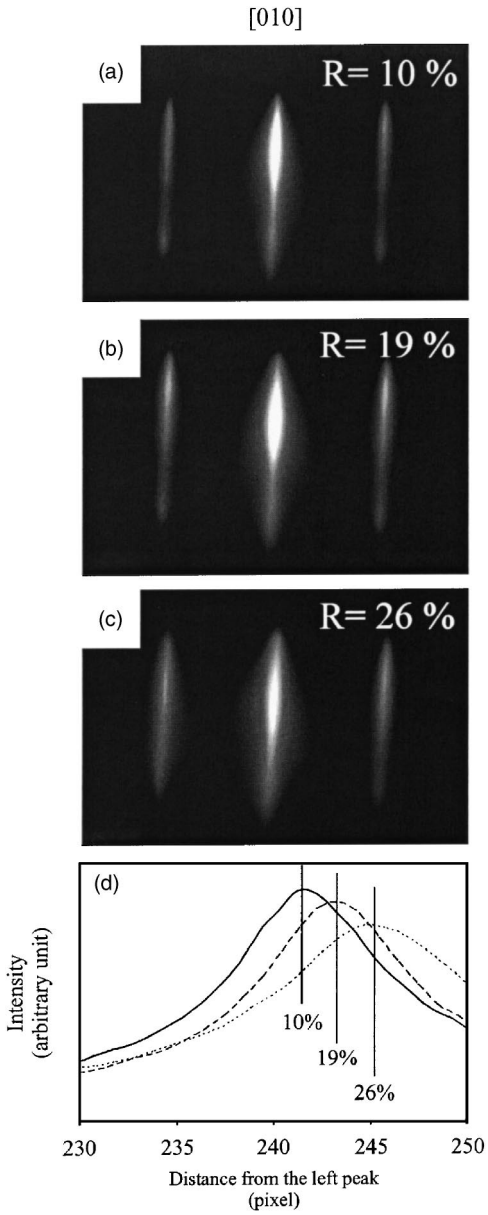

FIG. 6. (a)–(c) RHEED patterns of MnScN alloys grown at T_S=518 °C at different Mn/(Mn+Sc) flux ratios; (d) the average line profiles of the right (1 0) streak as a function of the distance from the midpoint of the corresponding left (−1 0) streak; the solid, dashed, and dotted lines are for RHEED patterns shown in (a), (b), and (c), respectively.

is calculated. In fact, both the *in-plane* and *out-of-plane* lattice constants of the MnScN alloy, a_{alloy} and c_{alloy}, are used to calculate the Mn fraction in the bulk, x_a and x_c, respectively, as

$$x_a = \frac{(a_{\text{ScN}} - a_{\text{alloy}})}{(a_{\text{ScN}} - a_{\text{MnN}})}, \tag{3}$$

$$x_c = \frac{(c_{\text{ScN}} - c_{\text{alloy}})}{(c_{\text{ScN}} - c_{\text{MnN}})}. \tag{4}$$

Figure 7(a) shows x_a and x_c as a function of R. The x_a values are calculated from the lateral spacing, a_{alloy}, using a_{ScN}=4.503 Å, as reported by Dismukes, Yim, and Ban, and a_{MnN}=4.22 Å, as reported by Yang *et al.*[3,23] Moreover, the x_c values are calculated from the vertical lattice constant of the

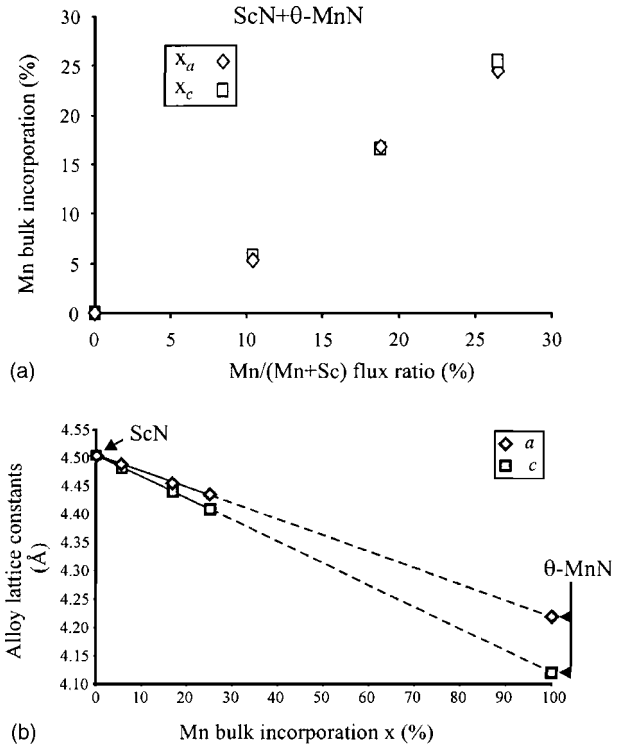

FIG. 7. (a) Mn bulk fraction in the alloy, x_a and x_c, calculated from Eqs. (3) and (4) as a function of Mn/(Mn+Sc) flux ratio; (b) The in-plane and out-of-plane lattice constants, a and c, respectively, of MnScN alloy as a function of the Mn bulk fraction; the dashed lines are the extrapolations of our experimental results which gives the expected lattice constants of the alloy for any Mn bulk concentration.

alloy, c_{alloy}, using the same lattice constant of ScN, $a_{\text{ScN}}=c_{\text{ScN}}$[23] and c_{MnN}=4.1287 Å.[3] As noticed, both x_a and x_c, calculated by RHEED and XRD, agree with each other within a small difference, less than 2.3%. Therefore, this shows that the alloy forms a continuous fct $Mn_xSc_{1-x}N$ phase.

In fact, applying Vegard's law, assuming the lattice constants of η-Mn_3N_2, $a_{Mn_3N_2}$=4.21 Å and $c/3_{Mn_3N_2}$=4.04 Å,[3] has been examined; however, there is a large difference between x_c and x_a in that case. For example, for the film grown at R=19%, the difference between calculated x_a and x_c is about 12%. The lack of good agreement using the M_3N_2 lattice parameters shows that these MnScN layers contain very few N vacancies, which are common for Mn_3N_2.

The Mn incorporation coefficient x/R for films grown with R=10%, 19%, and 26% are 0.54, 0.89, and 0.95, respectively. In fact, as seen in Fig. 7(a), both x and x/R increase as R increases.

Due to the fact that Mn/(Mn+Sc) bulk ratio x is always less than the Mn/(Mn+Sc) flux ratio R, it suggests that the accumulates mainly consist of Mn or MnN. However, for growth at T_S=330 °C, the accumulates may also contain Sc due to the reduced surface diffusion and possibility of increased surface-metal intermixing.

Figure 7(b) shows the alloy lattice constants, a and c, as a function of the Mn bulk incorporation x. The lattice constants at x=0 and 100% are the values known for ScN and θ-phase MnN, respectively. The data points are the lattice

constants measured for the films, so the interpolations, the dashed lines, indicate the expected lattice constants of $Mn_xSc_{1-x}N$ for $0.25<x<1$.

Qualitatively, the samples show a gradual darkening with increasing Mn incorporation, x. Furthermore, using a hot probe measurement, all films show n-type behavior, as does ScN grown in our system.[35] More detailed studies of the optical, electronic, and magnetic properties of MnScN have yet to be performed.

IV. SUMMARY

MnScN(001) alloys have been grown by rf MBE on ScN(001)/MgO(001) substrates. Structural measurements combined together, XRD and RHEED, show that MnScN has a fct structure having $a_{\text{alloy}}=b_{\text{alloy}}\neq c_{\text{alloy}}$. The growth is nearly optimized at $T_S=518\ ^\circ\text{C}$ for high Mn incorporation coefficient and smooth surface having fewer dot-like structures. The lattice parameters decrease as x increases. The MnScN lattice constants a and c both follow Vegard's law based on the lattice constants of ScN and θ-phase MnN. Mn incorporation and Mn incorporation coefficient at $T_S=518\ ^\circ\text{C}$ increase as Mn/(Mn+Sc) flux ratio increases. Given the good growth behavior, and easy incorporation, of Mn in ScN, a wide range of Mn concentrations is possible.

ACKNOWLEDGMENTS

The authors gratefully acknowledge the National Science Foundation for support (Grants Nos. 9983816 and 0304314). H. AL-Brithen also thanks King Saud University, Saudi Arabia for providing a scholarship.

[1]T. Dietl, H. Ohno, F. Matsukura, J. Cibert, and D. Ferrand, Science **287**, 1019 (2000).
[2]K. Suzuki, T. Kaneko, H. Yoshida, Y. Obi, H. Fujimori, and H. Morita, J. Alloys Compd. **306**, 66 (2000).
[3]H. Yang, H. Al-Brithen, E. Trifan, D. C. Ingram, and A. R. Smith, J. Appl. Phys. **91**, 1053 (2002).
[4]H. Shimizu, M. Shirai, and N. Suzuki, J. Phys. Soc. Jpn. **66**, 3147 (1997).
[5]M. B. Haider *et al.*, J. Appl. Phys. **93**, 5274 (2003).
[6]D. Gall, I. Petrov, N. Hellgren, L. Hultman, J. E. Sundgren, and J. E. Greene, J. Appl. Phys. **84**, 6034 (1998).
[7]J.-E. Sundgren, B. O. Johansson, A. Rockett, S. A. Barnett, and J. E. Greene, *Physics and Chemistry of Protective Coatings*, American Institute of Physics Series Vol. 149, edited by J. E. Greene, W. D. Sproul, and J. A. Thornton (AIP, New York, 1986), p. 149.
[8]H. Yang, H. Al-Brithen, A. R. Smith, J. A. Borchers, R. L. Cappelletti, and M. D. Vaudin, Appl. Phys. Lett. **77**, 3860 (2001).
[9]G. Kreiner and H. Jacobs, J. Alloys Compd. **183**, 345 (1992).
[10]W. R. Lambrecht, M. Prikhodko, and M. S. Miao, Phys. Rev. B **68**, 174411 (2003).
[11]W. R. Lambrecht1, Phys. Rev. B **62**, 13538 (2000).
[12]C. Stampfl, W. Mannstadt, R. Asahi, and A. J. Freeman, Phys. Rev. B **63**, 155106 (2001).
[13]H. A. Al-Brithen, E. M. Trifan, D. C. Ingram, A. R. Smith, and D. Gall, J. Cryst. Growth **242**, 345 (2002).
[14]A. R. Smith, H. A. H. Al-Brithen, D. C. Ingram, and D. Gall, J. Appl. Phys. **90**, 1809 (2001).
[15]D. Gall, I. Petrov, L. D. Madsen, J. E. Sundgren, and J. E. Greene, Vac. Sci. Technol. **A 16**, 2411 (1998).
[16]D. Gall, I. Petrov, P. Desjardins, and J. E. Greene, J. Appl. Phys. **86**, 5524 (1999).
[17]D. Gall, M. Stdele, K. Jrrendahl, I. Petrov, P. Desjardins, R. T. Haasch, T.-Y. Lee, and J. E. Greene, Phys. Rev. B **63**, 125119 (2001).
[18]N. Takeuchi, Phys. Rev. B **65**, 045204 (2002).
[19]B. Eck, R. Dronskowski, M. Takahashi, and S. Kikkawa, J. Mater. Chem. **9**, 1527 (1999).
[20]J.-E. Sundgren, B. O. Johansson, A. Rockett, S. A. Barnett, and J. E. Greene, in *Physics and Chemistry of Protective Coatings*, American Institute of Physics Series Vol. 149, edited by J. E. Greene, W. D. Sproul, and J. A. Thornton, (AIP, New York, 1986), p. 149.
[21]D. Gall, M. Stoehr, and J. E. Greene, Phys. Rev. B **64**, 174302, (2001).
[22]M. Little and M. E. Kordesch, Appl. Phys. Lett. **78**, 2891 (2001).
[23]J. P. Dismukes, W. M. Yim, and V. S. Ban, J. Cryst. Growth **13/14**, 365 (1972).
[24]H. A. AL-Brithen, A. R. Smith, and D. Gall, Phys. Rev. B **70**, 045303 (2004).
[25]X. Bai and M. E. Kordesch, Appl. Surf. Sci. **175-176**, 499 (2001).
[26]X. Bai, Doctoral Dissertation, Ohio University, 2002.
[27]W. Lengauer, J. Solid State Chem. **76**, 412 (1988).
[28]H. A. AL-Brithen and A. R. Smith, Appl. Phys. Lett. **77**, 2485 (2000).
[29]H. Munekata, H. Ohno, S. von Molnar, A. Segmüller, L. L. Change, and L. Esaki, Phys. Rev. Lett. **63**, 1849 (1989).
[30]H. Chen, A. R. Smith, R. M. Feenstra, D. W. Greve, and J. E. Northrup, MRS Internet J. Nitride Semicond. Res. **4S1**, G9.5 (1999).
[31]E. Haus, I. Smorchkova, B. Heying, P. Fini, C. Poblenz, T. Mates, U. Mishra, and J. Speck, J. Cryst. Growth **246**, 55 (2002).
[32]A. -L. Barabási and H. E. Stanley, *Fractal Concepts in Surface Growth* (Cambridge University Press, Cambridge, 1995), p. 133.
[33]T. Zywietz, J. Neugebauer, and M. Scheffler, Appl. Phys. Lett. **73** 487 (1998).
[34]RHEED for both ScN and MnScN was acquired at the growth temperature of the alloy, $T_S=518\ ^\circ\text{C}$, and room-temperature ScN lattice constant is used to extract the in plane room-temperature MnScN lattice constant assuming a very small difference between the thermal expansion coefficients of ScN and MnScN.
[35]Dieter K. Schroder, *Semiconductor Material and Device Characterization* (Wiley, New York, 1990), p. 30.